Hidden chains of optical vortices generated using a corner of phase wedge

Fadeyeva Tatyana A. [1, 2]

[1] Taurida National V. I. Vernadsky University, 4 Vernadsky Ave., 95007 Simferopol, Ukraine
[2] Institute of Physical Optics, 23 Dragomanov St., 79005 Lviv, Ukraine, e-mail: tatyana.fadeyeva@gmail.com

Received: 25.12.2012

Abstract. In the framework of paraxial approximation we consider evolution of a monochromatic Gaussian beam diffracted by a corner formed by three verges of the phase wedges of different types and the π-phase plate. We have found that the edges of the phase wedge generate macroscopic chains of identical optical vortices that disappear at the far field zone. At the same time, the π-phase plate can reproduce a very complex wave field whose structure depends on the scale of observation. At large scales there appear two π-cuts resembling broken edge dislocations with perpendicular directions. At small (some microns) scales two short vortex chains consisting of alternating-sign optical vortices are nucleated near the corner of the wedge. The analysis shows that the sizes of the chains decrease quickly when approaching the wedge surface. This enables us to assume that the π-phase plate can create so-called optical quarks in the evanescent waves of the edge field.

Key words: phase wedge, optical vortex, optical quark

PACS: 42.50.Tx
UDC: 535.1

1. Introduction

It is well known [1] that the diffraction process reproduces geometry of the edges of obstacle that scatters incident monochromatic beam. For example, a straight edge of a slab-sided phase plate begets a set of rectilinear diffracted maxima and minima parallel to the edge. However, even a very small disturbance of slab-sidedness leads inevitably to breaking the former symmetry down. There appears a new, hidden symmetry of the diffracted field, structural sells of which are optical vortices. Indeed, a slab-sided phase plane turns into a phase wedge, while the rectilinear diffracted maxima and minima are transformed into chains of optical vortices along the wedge brink [2–4]. The nature of such threaded vortex structure is rather simple. The brink of the wedge tears the wavefront out, whereas the slope of the wedge medium entails smooth phase changing. If we go around some axis perpendicular to the wedge base, though passing through the wedge brink along a closed contour, we will find that the phase incursion can reach the value 2π at a definite contour radius. This is a necessary condition for nucleating an optical vortex with an integer topological charge at the corresponding site of the wavefront in the propagating beam. Since the extension of the wavefront is much larger than the wavelength of the incident light, a whole chain of identical optical vortices will spring up at the wave zone of the diffracted beam.

Generally speaking, the phase wedge can be treated as an involute of a spiral phase plate [2] for generating optical vortices. However, such an involute presupposes a presence of all four edges of the wedge. It is these edges that bring additional perturbations into the symmetry of the dif-

fracted beams in the shape of hidden chains of the optical vortices. As a rule, such additional vortex chains can stretch over comparatively short lengths (several wavelengths), being got lost in the general diffraction pattern.

However, sometimes they come to the foreground, breaking the basic diffraction pattern down. This takes place, e.g., when the optical vortices with fractional topological charges are generated. Some fragments of this phenomenon have been considered by Berry [5] on the example of a spiral wave plate with a fractional topological charge. The fact is that the spiral phase plate with the phase step being equal to a multiple of 2π is intended for shaping integer-order optical vortices [6]. It would have been logical to assume that the spiral phase plate could generate the fractional-order optical vortices. As far back as in 1995 Soskin has shown [7] that computer-generated optical vortices can bear fractional topological charges, though remaining structurally unstable, while Berry [6] has described destruction of the fractional-order vortices into chains of integer-order optical vortices in the Gaussian beam evolving in the free space. Recently it has been shown that the phase singularities can nevertheless exist at sufficiently large distances in so-called error-function beams [8].

The aim of the present study is to trace the evolution of the vortex chains in the beam diffracted by the edges of the optical wedge, including the angles of slab-sided phase plates, which originate from nucleation of the fractional-order optical vortices.

2. Gaussian beam diffracted by the phase wedge

Let us consider a monochromatic Gaussian beam passing through a transparent dielectric phase wedge (with the refractive index n_w) lodged in a vacuum as shown in Fig. 1a, b and c. The phase wedge is characterised by the two angles α and β and the basic height h. The axis of the Gaussian beam is directed along the verge of the wedge.

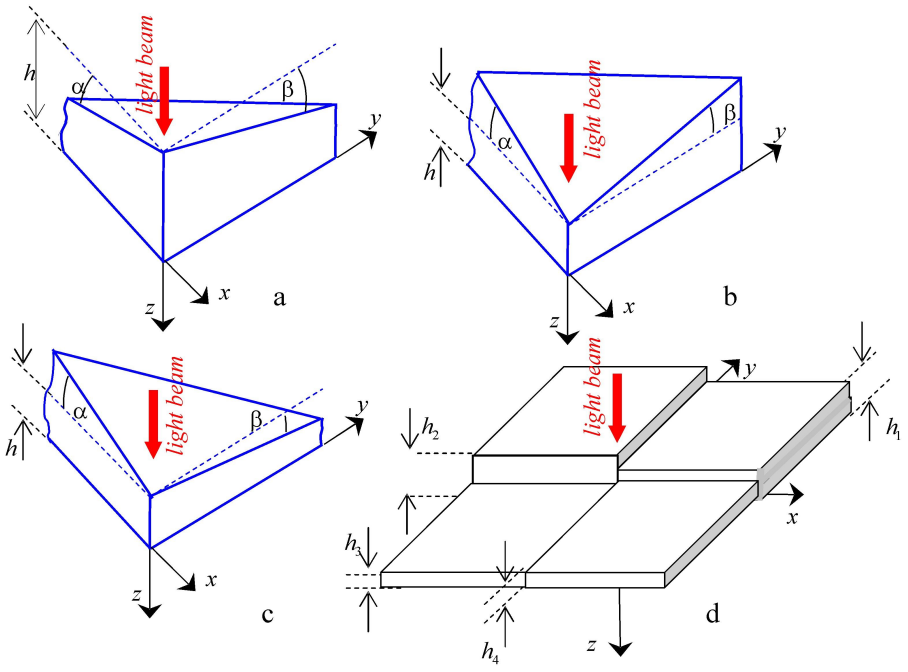

Fig. 1 Different types of phase wedges: (a) $\alpha, \beta > 0$, (b) $\alpha, \beta < 0$, (c) $\alpha > 0, \beta < 0$, and (d) composite step-phase plate.

The field diffracted by the wedge can be described in the paraxial approximation in terms of the Fresnel diffractive integral [1]:

$$\Psi(x,y,z) = A\frac{\exp\{-ikz\}}{z}\int\limits_{-\infty}^{\infty}\int\limits_{-\infty}^{\infty} dx'dy'\,\Psi_0(x',y') \times \exp\left\{-i\frac{k}{2z}\left[(x-x')^2+(y-y')^2\right]\right\}, \quad (1)$$

where A is a constant, k stands for the wavenumber in the free space, and x and y are the transverse coordinates at the observation plane.

The field Ψ_0 an the initial plane $z=0$ may be written as

$$\Psi(x',y') = \exp\left\{-\frac{x'^2+y'^2}{w_0^2}\right\} \times \exp\left\{-ik\left(\left[n(x',y')-1\right]\left[x'\tan\alpha + y'\tan\beta\right] + d(x',y')\right)\right\}, \quad (2)$$

with

$$n(x,y) = \begin{cases} n_w, & x<0, y>0 \\ 1, & x>0; x<0, y<0 \end{cases}, \quad (3)$$

$$d(x',y') = \begin{cases} (n_w-1)h, & x'<0, \quad y'>0 \\ 0, & x'>0;\ x'<0,\ y'<0 \end{cases}, \quad (4)$$

where w_0 stands for the beam waist at the plane $z = 0$, and α and β are the slope angles of the wedge sides along the x and y axes, respectively.

After integration we obtain

$$\Psi(x,y,z) = \frac{A'}{\sigma}\exp\left\{-\frac{x^2+y^2}{w_0^2\sigma} - ikz\right\}\left[\operatorname{erfc}\left(\sqrt{\frac{ik}{2z\sigma}}y\right) + \frac{1}{2}\operatorname{erfc}\left(-\sqrt{\frac{ik}{2z\sigma}}x\right)\operatorname{erfc}\left(-\sqrt{\frac{ik}{2z\sigma}}y\right) + \frac{1}{2}\exp(-i\Delta\Phi)\operatorname{erfc}\left(\sqrt{\frac{ik}{2z\sigma}}[x-Cz]\right)\operatorname{erfc}\left(-\sqrt{\frac{ik}{2z\sigma}}[y-Fz]\right) \times \exp\left\{-i\frac{k\left[F(2y-Fz)+C(2x-Cz)\right]}{2\sigma}\right\}\right], \quad (5)$$

where A' is constant, $F = (n_w-1)\tan\beta$, $C = (n_w-1)\tan\alpha$, $\Delta\Phi = k(n_w-1)d$ is the phase difference between the portions of the beam passing respectively though the wedge and the free space, $\operatorname{erfc}(X)$ is the complimentary error function [9] ($\operatorname{erfc}(X) = 1-\operatorname{erf}(X)$, with $\operatorname{erf}(X) = \frac{2}{\sqrt{\pi}}\int\limits_0^X e^{-t^2}dt$ standing for the error function), $\sigma = 1 - iz/z_0$, and $z_0 = kw_0^2/2$ is the Rayleigh length in the free space. Besides, we have made use of the integrals (see [10])

$$\int\limits_{-\infty}^{\infty}\exp\left\{-px^2-qx\right\}dx = \sqrt{\frac{\pi}{p}}\exp\left\{\frac{q^2}{4p}\right\}, \quad (6)$$

$$\int\limits_{0}^{\infty}\exp\left\{-px^2-qx\right\}dx = \frac{1}{2}\sqrt{\frac{\pi}{p}}\exp\left\{\frac{q^2}{4p}\right\}\operatorname{erfc}\left(\frac{q}{2\sqrt{p}}\right). \quad (7)$$

Eq. (5) shows that we deal in fact with five principal waves: two waves are reflected by the wedge along the *x* and *y* directions, one of them passes through the free space, and the remaining

two are boundary waves diffracted by the two wedge brinks. Typical diffraction patterns for different wedges (see Fig. 1a, b and c) are shown in Fig. 2 and Fig. 3. Far from the verge of the wedge (at $x = y = 0$), the diffraction pattern is shaped by only three waves: a free propagating wave, a reflected one, and a boundary wave diffracted by the wedge brink (at either $x = 0$ or $y = 0$). We observe here two sets of identical optical vortices along the brinks of the wedge. The principal condition for shaping a vortex is that the pass-by along a circle of radius r_0 around the vortex axis must get the phase incursion equal to 2π [2]. In fact, the boundary wave forms a set of parallel lines of equal phases and amplitudes. The two other waves also form a set of such lines which are inclined at some angle with respect to the first ones. The vortex is nucleated when the amplitudes of these two wave combinations are the same and the phase difference is equal to π. However, the mutual tilt of the equiphase lines results in perturbing the vortex form, the vortex becoming the elliptical one. In order to flatten the vortex shape, the radius r_0 of the pass-by and the beam waist radius w_0 are to be equal to each other [3].

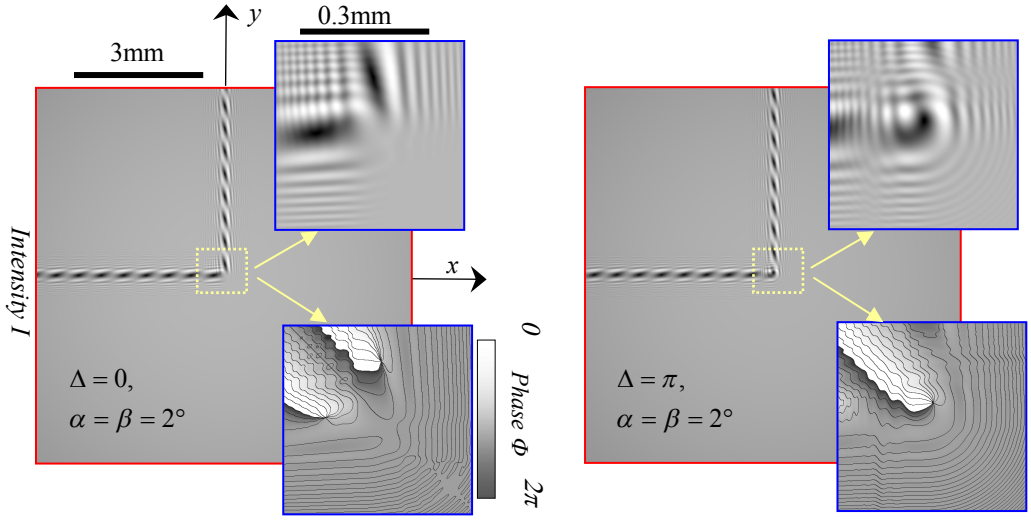

Fig. 2. Distributions of intensity *I* and phase Φ after diffraction of the Gaussian beam by the phase wedge with the equal angles $\alpha = \beta$ between the verges (*z* = 0.1 mm and $w_0 = 1$ mm).

The structure of the beam field near the verge (at $x = y = 0$) is defined by the phase $\Delta\Phi$ and the signs of the angles α and β (see the framed patterns in Fig. 2 and Fig. 3). This may be represented as

$$\Psi(x \to 0, y \to 0, z) = \frac{A}{\sigma}\exp\left\{-\frac{x^2+y^2}{w_0^2\sigma} - ikz\right\}\left[\frac{3}{2} - \frac{1}{2}\sqrt{\frac{ik}{\pi z\sigma}}y + \frac{1}{2}\sqrt{\frac{ik}{\pi z\sigma}}x\right.$$
$$+\frac{1}{2}\exp(-i\Delta\Phi)\left(1-\sqrt{\frac{ik}{\pi z\sigma}}[x-Cz]\right), \quad (8)$$
$$\left.\times\left(1+\sqrt{\frac{ik}{\pi z\sigma}}[y-Fz]\right)\exp\left\{-i\frac{k[F(2y-Fz)+C(2x-Cz)]}{2\sigma}\right\}\right]$$

where we have used the approximation $\mathrm{erfc}(X) = 1 - \sqrt{2\pi}X$, $X << 1$ [9].

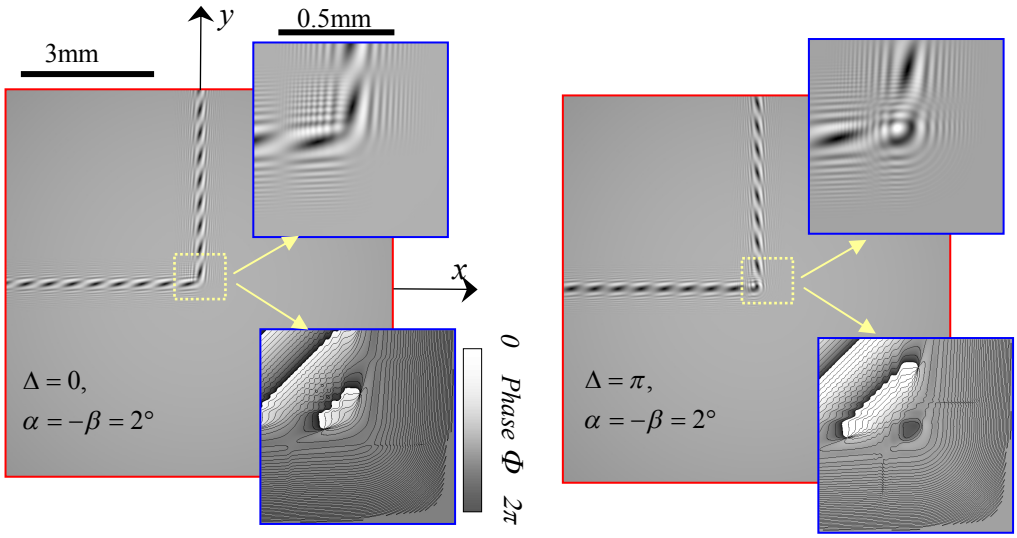

Fig. 3. Distributions of intensity *I* and phase Φ after diffraction of the Gaussian beam by the phase edge with the opposite signs of the angles $\alpha = -\beta$ between the verges (*z* = 0.1 mm and $w_0 = 1$ mm).

When the phase difference is $\Delta\Phi = 0$ and the angles are the same ($\alpha = \beta$), there is no singly charged vortex near the axis *z* = 0. Instead, we observe here two symmetrically positioned optical vortices with the same topological charges. However, when the phase difference is $\Delta\Phi = \pi$, we obtain a single optical vortex near the axis *z* = 0. On the other hand, when the wedge has the angles with different signs $\alpha = -\beta$, a single optical vortex is not nucleated under the both conditions $\Delta\Phi = 0$ and $\Delta\Phi = \pi$ (see Fig. 3). Instead, there appears a topological dipole with two oppositely charged optical vortices in the vicinity of the verge.

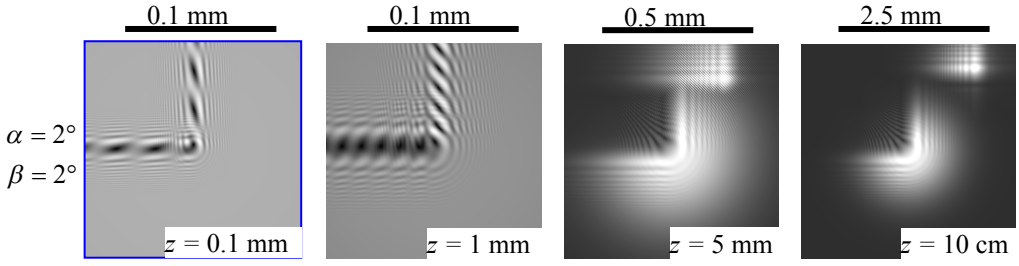

Fig. 4. Spatial evolution of diffracted Gaussian beam by the phase wedge ($w_0 = 1$ mm).

Propagation of the beam is accompanied by essential perturbation of diffraction pattern shown in Fig. 4. If we observe the vortex chains along the brinks *x* and y (see Fig. 4; *z* = 1 mm) at the wave zone, then the vortex chains vanish at the far field (see Fig. 4; *z* = 5 mm and *z* = 10 cm). At the same time, there appears an additional diffractive image of the wedge in the upper right corner. Such an additional image is shaped by the two principal reflected waves (there is no free propagating wave there). On the other hand, two boundary waves forms the pattern of short, strongly perturbed chains of optical vortices in the vicinity of the verge (*x* = *y* = 0) in the lowest pattern.

3. Slab-sided and combined phase plates

3.1. Slab-sided phase plate

An ordinary slab-sided phase plate is a habitual optical element used, as a rule, in optical interferometers or similar devices for introducing desirable phase differences. However, in our case the slab-sided phase plane manifests unusual properties. The diffracted field behind the plate can be obtained from Eq. (5) if the angles are equal to $\alpha = \beta = 0$:

$$\Psi(x,y,z) = \frac{A}{\sigma}\exp\left\{-\frac{x^2+y^2}{w_0^2\sigma} - ikz\right\}\left\{\operatorname{erfc}\left(\sqrt{\frac{ik}{2z\sigma}}y\right) - \operatorname{erf}\left(\sqrt{\frac{ik}{2z\sigma}}x\right)\operatorname{erfc}\left(-\sqrt{\frac{ik}{2z\sigma}}y\right)\right\}, \tag{8}$$

where the relation $\Delta\Phi = \pi$ is assumed (i.e., we will deal with the π-phase plate later on). We obtain

$$\Psi(x,y,z) = \frac{A}{\sigma}\exp\left\{-\frac{x^2+y^2}{w_0^2\sigma} - ikz\right\}\left\{1 - \operatorname{erf}\left(\sqrt{\frac{ik}{2z\sigma}}y\right) - \operatorname{erf}\left(\sqrt{\frac{ik}{2z\sigma}}x\right)\left[1 + \operatorname{erf}\left(\sqrt{\frac{ik}{2z\sigma}}y\right)\right]\right\}. \tag{9}$$

A typical pattern for the Gaussian beam diffracted by the verge $x = y = 0$ of the π-phase plate is shown in Fig. 5. It seems at the first glance that the black lines along the brinks $x = 0$ and $y = 0$ of the plate are two broken edge dislocations with orthogonal directions and the origin located at the point $x = y = 0$. However, the beam field at a small scale (see the framed pictures in Fig. 5) turns out to be of a complicated singular structure. There are two short vortex chains near the beam axis. The distance between two neighbouring vortices shortens quickly as the coordinates along the *x* and *y* axes increase. The vortex chains vanish far from the beam axis and the equiphase lines smooth gradually out. *This means that the π-phase plate can never introduce the exact π-phase shift into the beam (i.e., an edge dislocation), even in a purely theoretical case*. The latter represents a result of the edge effect.

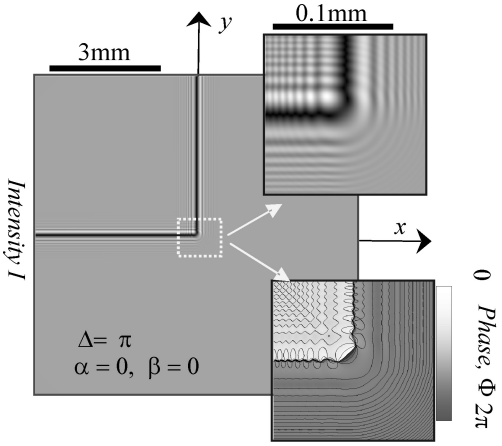

Fig. 5. Distributions of intensity *I* and phase Φ after diffraction of the Gaussian beam by the π-phase plate ($\alpha = \beta = 0$ and $\Delta\Phi = \pi$).

When the beam is propagating, the singular structure does not change, as shown in Fig. 6. The observable variations of the field structure for the evolving beam are due to changing transverse field scale, whereas the solid angle of the beam divergence remains constant. In contrast to the phase wedge, near the axis of the π-phase plate we observe a structurally stable topological

dipole consisting of two oppositely charged optical vortices. The field structure of such a wave construction is shown in Fig. 7. One can notice that the study [11] has presented simple experimental results for the Gaussian beam diffracted by the π-phase plate.

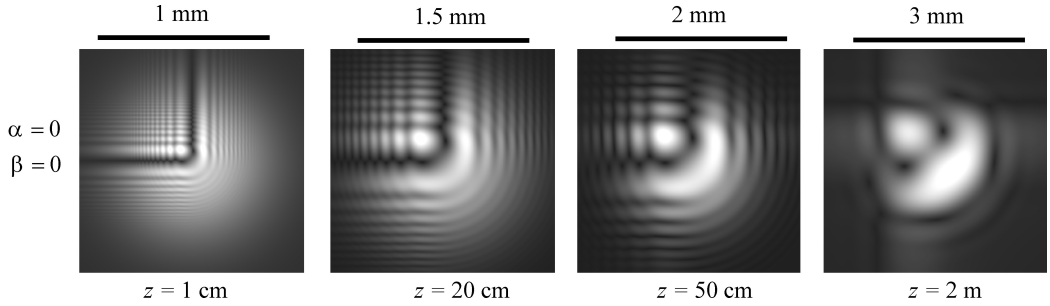

Fig. 6. Evolution of singular structure along the Gaussian beam diffracted by the π-phase plate ($w_0 = 0.5$ mm).

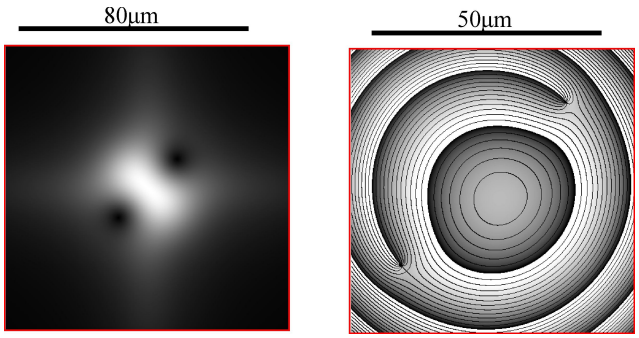

Fig. 7. Structurally stable topological dipole generated by the π-phase plate ($\alpha = \beta = 0$, $w_0 = 30$ μm and $z = 50$ μm).

3.2. Composite phase plate

As shown above, the π-phase plate introduces two perpendicular cuts in the initial wavefront. However, this device cannot make only one π-cut in the beam, though such an operation can be performed by a composite slab-sided phase plates shown in Fig. 1d. In this case Eq. (5) may be reconstructed to the following form:

$$\Psi(x,y,z) = \frac{A}{\sigma}\exp\left\{-\frac{x^2+y^2}{w_0^2\sigma} - ikz\right\}$$
$$\times\left\{\operatorname{erfc}\left(-\sqrt{\frac{ik}{2z\sigma}}x\right)\left[\operatorname{erfc}\left(-\sqrt{\frac{ik}{2z\sigma}}y\right)\exp\left(-i\Phi_1\right)+\operatorname{erfc}\left(\sqrt{\frac{ik}{2z\sigma}}y\right)\exp\left(-i\Phi_4\right)\right]\right. \quad , \qquad (10)$$
$$\left.+\operatorname{erfc}\left(\sqrt{\frac{ik}{2z\sigma}}x\right)\left[\operatorname{erfc}\left(-\sqrt{\frac{ik}{2z\sigma}}y\right)\exp\left(-i\Phi_2\right)+\operatorname{erfc}\left(\sqrt{\frac{ik}{2z\sigma}}y\right)\exp\left(-i\Phi_3\right)\right]\right\}$$

where $\Phi_j = k\,h_j$ and $j = 1,2,3,4$.

The phase sequence Φ_j enables us to construct a wished shape of the combined phase plate. For example, the sequence $\Phi_1 = \pi/2$, $\Phi_2 = 0$, $\Phi_3 = 2\pi$ and $\Phi_4 = \pi$ makes only one π-cut in the initial wavefront. The corresponding field structure is illustrated by Fig. 8a. Here we have again a semblance of the broken edge dislocation at a large scale. However, a likeness of the re-

stricted edge dislocation turns into a short chain of optical vortices at smaller scales. The singly charged optical vortices are positioned near the beam axis.

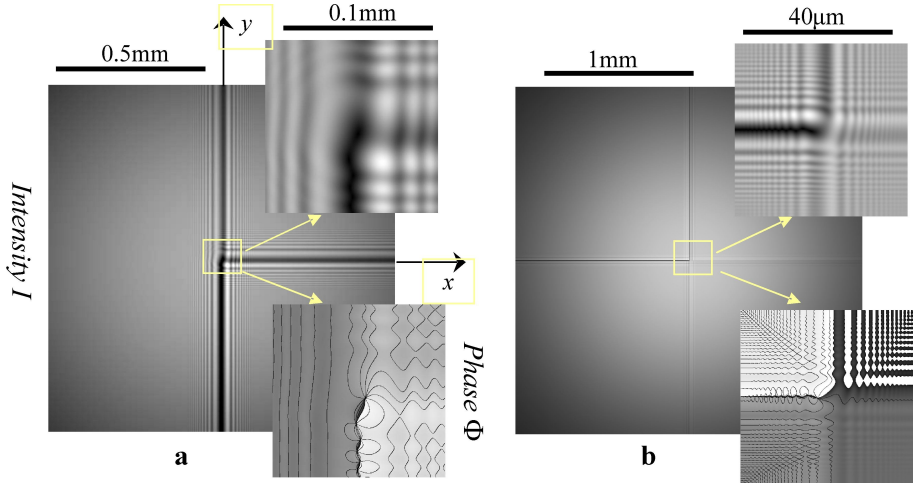

Fig. 8. Intensity and phase distributions in the beams with the π-cut: the pass-by with (a) 2π- and (b) π-phase incursions ($w_0 = 1$ mm and $z = 100$ μm).

Recently Volyar [12] has suggested an unusual wave construction in the form of a so-called optical quark. Such a beam can carry over an optical vortex with half-integer charge at the end of the broken edge dislocation. A sum of two quarks with the same signs of their topological indices but different parities can form singular beams with integer-order optical vortices, while the difference of these quarks form non-singular beams. A possible phase device for shaping such an optical quark may have the phase sequence $\Phi_1 = \pi/2$, $\Phi_2 = \pi$, $\Phi_3 = 0$, and $\Phi_4 = \pi/4$. The field distribution at a large scale has much to do with the optical quark (see Fig. 8b), but the field looks different at small scales. We meet again a very short vortex chain (20 μm lengthwise at $z = 100$ μm) with the singly charged optical vortex at the end, the vortex being shifted with respect to the beam axis.

The spatial evolution of the quark-like beam is shown in Fig. 9. As the beam propagates, the field structure is essentially reconstructed. The distance between optical vortices in the chain increases whereas the number of the visible vortices decreases.

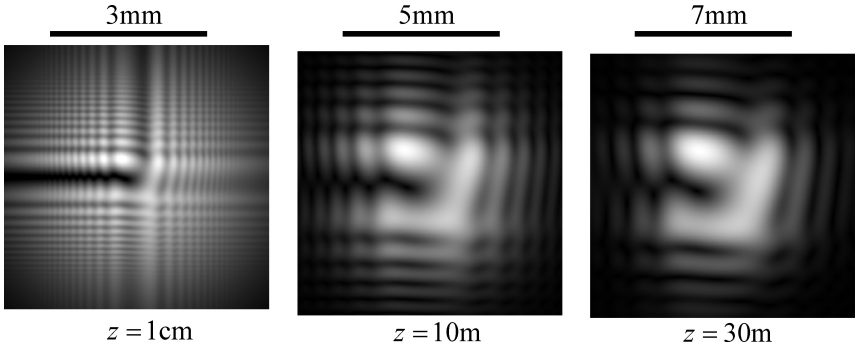

Fig. 9. Evolution of singular beam with the π-cut and the pass-by π ($w_0 = 1$mm).

In order to find the optimal conditions for shaping the optical quarks, it is necessary to analyse the structure of the vortex chain.

3.3. Structure of the vortex chain

Let us estimate the size of the vortex chain and the distance between the neighbouring vortices. A typical pattern of phase distribution in the vortex chain behind the π-phase plate is shown in Fig. 10. The positions of the vortex and the distances between them depend strongly on the position z of the observation plane. Nucleation of vortices in the chain is defined by the superposition edge waves diffracted by the x and y edges. The equiphase lines in Fig. 10 appear indirectly near the x-edge, though the vortices do not lodge along the straight line, choosing the places corresponding to the same amplitudes and the π-phase difference. For that reason there are no optical vortices far from the plate edges. The same reason defines the infinite sizes of the vortex chain: the amplitude of one of the waves remains nearly constant, while the amplitude of the other decreases. It is the amplitude variations diffracted by the y-edge that result in nucleating the vortex chain along the x-edge. The amplitude variations are caused by the error function in Eq. (8). Let us analyse some properties of that function. Fig. 11 illustrates behaviour of the amplitude and phase of the error function $y = \mathrm{erf}\left(\sqrt{i}\,x\right)$ with varying complex argument. The amplitude oscillates near the value $\mathrm{abs}\,y = 1$, whereas the phase difference between the positive and negative values x is equal to π.

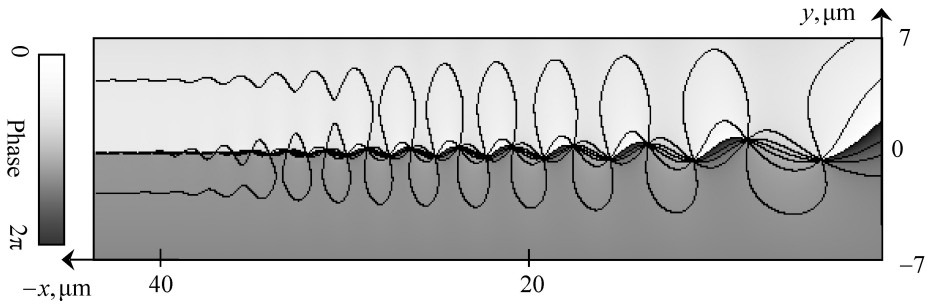

Fig. 10. Phase distribution and equiphase lines of vortex chain near the x-edge of the π-phase plate ($w_0 = 1\mathrm{mm}$ and $z = 0.1\mathrm{mm}$).

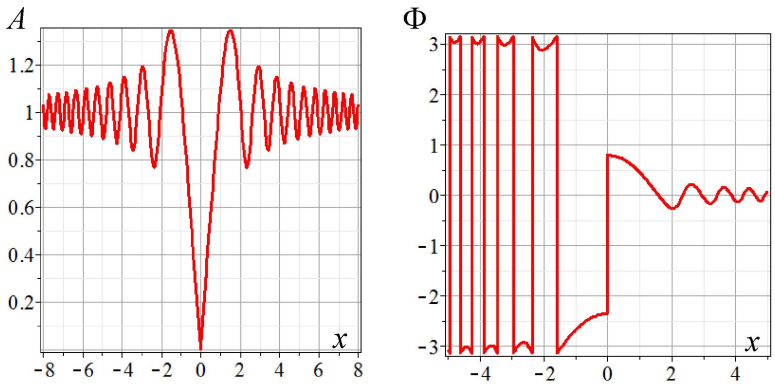

Fig. 11. Amplitude A and phase Φ of the error function $\mathrm{erf}\left(\sqrt{i}\,x\right)$ of complex argument.

The shape of oscillations of the curve depicted in Fig. 11 means that the error function should be written in terms of trigonometric functions. Let us now separate the real and imaginary parts of that function. The corresponding relation is as follows [9]:

$$\operatorname{erf}\left[\frac{\sqrt{\pi}}{2}(1+i)X\right]=C(X)-iS(X), \tag{11}$$

with the Fresnel cosine and sine functions

$$C(X)=\int_0^X\cos\left(\frac{\pi}{2}t^2\right)dt\,,\ S(X)=\int_0^X\sin\left(\frac{\pi}{2}t^2\right)dt\,, \tag{12}$$

X being the real variable, and $C(X)$ and $S(X)$ standing for the Fresnel cosine and sine, respectively.

In its turn, the Fresnel cosine and sine may be expressed in terms of the trigonometric and Bessel functions as

$$C\left(\sqrt{\frac{2x'}{\pi}}\right)=\sqrt{2}\left[\cos\frac{x'}{2}\sum_{n=0}^{\infty}(-1)^nJ_{2n+\frac{1}{2}}\left(\frac{x'}{2}\right)+\sin\frac{x'}{2}\sum_{n=0}^{\infty}(-1)^nJ_{2n+\frac{3}{2}}\left(\frac{x'}{2}\right)\right], \tag{13}$$

$$S\left(\sqrt{\frac{2x'}{\pi}}\right)=\sqrt{2}\left[\sin\frac{x'}{2}\sum_{n=0}^{\infty}(-1)^nJ_{2n+\frac{1}{2}}\left(\frac{x'}{2}\right)-\cos\frac{x'}{2}\sum_{n=0}^{\infty}(-1)^nJ_{2n+\frac{3}{2}}\left(\frac{x'}{2}\right)\right], \tag{14}$$

where $J_{2n+\frac{1}{2}}\left(\frac{x}{2}\right)$ is the Bessel function of the half-integer order and the first kind. Thus, we get

$$C\left(\sqrt{\frac{2x'}{\pi}}\right)-iS\left(\sqrt{\frac{2x'}{\pi}}\right)=\sqrt{2}\,e^{-i\frac{x'}{2}}\left[\sum_{n=0}^{\infty}(-1)^nJ_{2n+\frac{1}{2}}\left(\frac{x'}{2}\right)+i\sum_{n=0}^{\infty}(-1)^nJ_{2n+\frac{3}{2}}\left(\frac{x'}{2}\right)\right]. \tag{15}$$

On the other hand, the Bessel functions of the half-integer order are linked with the spherical Bessel functions j_n by the relation

$$j_n(\xi)=\sqrt{\frac{\pi}{2\xi}}J_{n+\frac{1}{2}}(\xi), \tag{16}$$

while the spherical Bessel functions may be presented in terms of the elementary trigonometric functions (see below):

$$C\left(\sqrt{\frac{2x'}{\pi}}\right)-iS\left(\sqrt{\frac{2x'}{\pi}}\right)=\sqrt{\frac{2x'}{\pi}}\,e^{-i\frac{x'}{2}}\left[\sum_{n=0}^{\infty}(-1)^nj_{2n}\left(\frac{x'}{2}\right)+i\sum_{n=0}^{\infty}(-1)^nj_{2n+1}\left(\frac{x'}{2}\right)\right]. \tag{17}$$

Besides, the definition of the spherical Bessel function is given by

$$j_n(x')=\frac{x'^n}{2^{n+1}n!}\int_0^{\pi}\cos(x'\cos\theta)\sin^{n+1}\theta\,d\theta\,. \tag{18}$$

This means that the function j_n is expressed by the sum of the trigonometric functions $\frac{\cos x'}{x'^m}$ and $\frac{\sin x'}{x'^m}$, where $m=0,1,2,...,n+1$. In our case we can restrict ourselves to the simplest estimation, so that we put $n=0$ in the above expression:

$$C\left(\sqrt{\frac{2x}{\pi}}\right)-iS\left(\sqrt{\frac{2x}{\pi}}\right)\sim\sqrt{\frac{2x}{\pi}}\,e^{-i\frac{x}{2}}\left\{j_0\left(\frac{x}{2}\right)+i\,j_1\left(\frac{x}{2}\right)\right\}. \tag{19}$$

The error of that estimation is about $O\left(\sqrt{x^{-3}}\right)$. Since we have

$$j_0(x') = \frac{\sin x'}{x'},\ j_1(x) = \frac{\sin x'}{x'^2} - \frac{\cos x'}{x'}, \tag{20}$$

we obtain from Eq. (19)

$$C\left(\sqrt{\frac{2x'}{\pi}}\right) - iS\left(\sqrt{\frac{2x'}{\pi}}\right) \sim -\frac{i2}{\sqrt{\pi}}\left\{\frac{1}{\sqrt{x'/2}} - \frac{e^{-ix/2}}{2\sqrt{2}}\frac{\sin(x'/2)}{\sqrt{(x'/2)^3}}\right\} \xrightarrow{x'\to 0} 0. \tag{21}$$

The second term in Eq. (21) is responsible for the oscillations and, consequently, for the nucleation of vortices in the chains in Eq. (10). As a matter of fact, Eq. (12) gives an adequate estimation only for $x' >> 1$ (i.e., far from the beam axis).

After relevant changes in the notations adopted in Eqs. (11) and (21), we arrive to the expression

$$erf\left[\frac{\sqrt{\pi}}{2}(1+i)X\right]\Big|_{X>>1} \sim -\frac{i2}{\sqrt{\pi}}\left\{\frac{2}{X\sqrt{\pi}} - \frac{e^{-i\frac{\pi}{4}X^2}}{2\sqrt{2}}\frac{\sin\left(\frac{\pi}{4}X^2\right)}{X^3\sqrt{\left(\frac{\pi}{4}\right)^3}}\right\}. \tag{22}$$

By comparing Eq. (22) with the error functions in Eq. (10) and assuming that $z << z_0$ (the paraxial approximation at the wave zone) and $\sigma \approx 1$, we obtain

$$\mathrm{erf}\left(\sqrt{\frac{ik}{2z}}x\right)\Big|_{x>>\sqrt{\frac{\pi z}{k}}} \sim -\frac{i2}{\sqrt{\pi}}\left\{\frac{2}{\sqrt{\frac{k}{z}}\,x} - \frac{e^{-i\frac{\pi k}{4z}x^2}}{2\sqrt{2}}\frac{\sin\left(\frac{\pi k}{4z}x^2\right)}{\sqrt{\left(\frac{k}{4z}\right)^3}\,x^3}\right\}. \tag{23}$$

Thus, the oscillations period corresponding to the vortex positions can be estimated as

$$\frac{\pi k}{4z}x^2 = 2\pi m,\ \ m = 1,2,3,\ldots. \tag{24}$$

The circles in Fig. 12 outline the distance between the neighbouring vortices in the chain. When the number of vortices increases, this distance gets shorter rapidly. However, the vortices do not annihilate in this case.

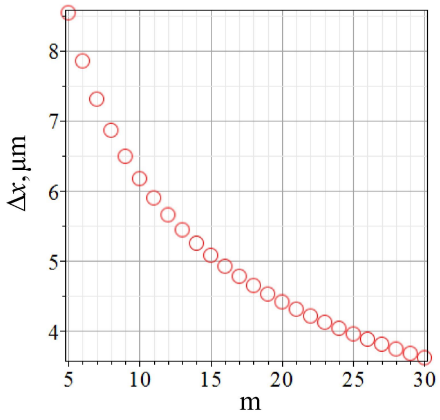

Fig. 12. Distance Δx between neighbouring vortices in the chain as a function of vortex number m ($z = 0.1$ mm).

The theoretical wave approach does not impose any restrictions on the distance between the vortices. The physical reason for the restricted vortex chain is caused by a loss of conditions for

the vortex nucleation because of essential difference between the two diffracted waves (the amplitude oscillations of the wave diffracted by the *y*-edge go down along the *x* axis as x^{-3} – see also Eq. (23)). Computer simulations testify that the length of the vortex chain at the wave zone is proportional to the square root of the distance z to the observation plane, just as for the distance between the vortices given by Eq. (24).

Rapid shortening of the length of the vortex chain at the edges of the π-phase plate with increasing distance to the observation plane $l \sim \sqrt{z/k}$ enables us to assume that the vortex chains would vanish at the near-field zone in the vicinity of the edges. In its turn, it also enables us to suppose that the optical quarks [12] can exist at the near-field zone, at least in the evanescent waves. However, a consistent analysis of this problem needs absolutely different physical approaches which go far beyond the scope of our present consideration.

Conclusions

In this study we have considered the evolution of the monochromatic Gaussian beam diffracted by the corner formed by three verges of the phase wedges of different types, using the paraxial approximation. When the angles of the wedge are zero, we deal with the ordinary phase plate. The structure of the diffracted field is strongly determined by the scale and the position of observer. As a rule, all types of the wedges produce chains of the identical optical vortices in the wave zone stretching along their edges. However, the properties of the optical vortex being nucleated near the wedge angle depend on the wedge parameters. The vortex chains disappear at the far-field zone, while a restricted set of the vortices near the wedge angle experiences essential perturbations. The fact is that the vortex pattern can be treated as a superposition of five principal local waves: the two waves reflected by the upper surface of the wedge, the free propagating wave, and the two edge waves diffracted by the wedge brinks. At the far-field zone, the two reflected waves form a separate lateral picture and do not take place in shaping the basic pattern, whereas the deformed angular vortex pattern inside the basic pattern is shaped by the two edge waves and the freely propagating local beam.

An altogether different situation occurs for the beam diffracted by the phase plate introducing the π-phase difference between the portions of the beam. At large scales we observe the field with two restricted π-cuts resembling two broken edge dislocations, with the perpendicular directions connected at the beam axis. However, at small scales (of the order of some microns) there appear short vortex chains along the wedge edges, with the singly charged optical vortices of alternating signs. A structurally stable topological dipole is observed at the wedge corner, of which shape does not change along the beam length. We have also analysed the field with only one 'broken edge dislocation', with the short vortex chain inside of it produced by the combined phase plate. The analysis of the chain structure has testified that the size of the chain is proportional to the square root of the distance from the wedge. When approaching the wedge, the chain length decreases very quickly and tends to zero. This circumstance makes reasonable the assumption that the corner of the π-phase plate may produce the so-called optical quarks in the evanescent waves.

Acknowledgement

The author thanks Professor A. V. Volyar for helpful discussions. The research has been partially supported by the State Fund for Fundamental Researches of Ukraine (the projects No 0111U008256; Ф41.1/010) and the Ministry of Education, Science, Youth and Sport of Ukraine (the project No 0112U000451; 296/12).

References

1. Born M and Wolf E, Principles of optics. New York: Pergamon (1975).
2. Izdebskaya Ya V, Shvedov V G and Volyar A V, 2004. Singular beam diffraction by the edge of a dielectric medium. Ukr. J. Phys. Opt. **5**: 96–99.
3. Volyar A V, Fadeeva T A and Shvedov V G, 2002. Optical vortex generation and Jones vector formalism. Opt. Spectrosc. **93**: 267–272.
4. Izdebskaya Ya, Shvedov V and Volyar A, 2005. Focusing of wedge-generated higher-order optical vortices. Opt. Lett. **30**: 2530–2532.
5. Berry M V, 2004. Optical vortices evolving from helicoidal integer and fractional phase steps. J. Opt. A. **6**: 259–269.
6. Beijrabergen M W, Coerwinkel R P C, Kristensen M and Woerdman J P, 1994. Helical-wavefront laser beams produced with a spiral phase plate. Opt. Commun. **112**: 321–327.
7. Basisty I, Soskin M and Vasnetsov M, 1995. Optical wavefront dislocations and their properties. Opt. Commun. **119**: 604–612.
8. Fadeyeva T, Alexeyev C, Rubass A and Volyar A, 2012. Vector erf-Gaussian beams: fractional optical vortices and asymmetric TE and TM modes. Opt. Lett. **37**: 1397–1399.
9. Abramowitz M and Stegun I A, Handbook of mathematical functions, 10th ed. Washington: NBS (1972).
10. Prudnikov A P, Brychkov Yu A and Marichev O I, Integrals and series, Vol. 1: Elementary functions. New York: Gordon and Breach (1986).
11. Kim G-H, Jeon J-H, Ko K-H, Moon H-J, Lee J-H and Chang J-S, 1997. Optical vortices produced with nonspiral phase plate. Appl. Opt. **35**: 8614–8621.
12. Volyar A V, 2013. Do optical quarks exist in the free space? A scalar treatment. Ukr. J. Phys. Opt. **14**: 31–43.

Fadeyeva Tatyana A., 2013. Hidden chains of optical vortices generated using a corner of phase wedge. Ukr.J.Phys.Opt. **14**: 57 – 69.

Анотація. *В рамках параксіального наближення в роботі розглянута еволюція монохроматичного гаусівського променя, дифрагованого на куті, сформованому трьома гранями клинів різного типу і π-фазової пластинки. Виявлено, що краї фазового клина генерують макроскопічний ланцюжок ідентичних оптичних вихорів, які зникають у далекій зоні. Разом з тим, π-фазова пластинка може репродукувати складну структуру хвильового поля, яка залежить від масштабу спостереження. У великих масштабах виникає два π-зрізи, які нагадують зламані крайові дислокації з перпендикулярними напрямками. При малих масштабах (кілька мікрон) два коротких ланцюжки вихорів з протилежними зарядами, які зароджуються біля клину. Як випливає з аналізу, розмір ланцюжків швидко зменшується при прямуванні до поверхні клину. Це дозволяє нам припустити, що π-фазова пластинка може створювати так звані оптичні кварки в еванесцентних хвилях на границі поля.*